Nanomaterials

DOI: 10.1002/ange.201101572

Ultrasmall Color-Tunable Copper-Doped Ternary Semiconductor Nanocrystal Emitters**

*Suresh Sarkar, Niladri S. Karan, and Narayan Pradhan**

Synthesis of light-emitting dispersed semiconductor nanocrystals with tunable emission has been widely studied in the last two decades because of their potential applications in photovoltaics, optoelectronics, and biology.[1] Soon after the development of high-quality CdSe nanocrystals with spectacular size-dependent tunable excitonic emission in the entire visible window,[2] simplification of the synthetic method,[3] stabilization of the emission,[4] surface functionalization of the nanocrystals,[5] design of non-cadmium nanocrystal emitters,[6] fabrication of different kinds of composition-tunable multifunctional alloy nanocrystals,[7] and related photophysical properties[8] have been widely investigated for both fundamental understanding and their implementation in day-to-day developing technology. Analysis of up to date literature reports reveals that biological applications require strongly emitting, small and nontoxic nanocrystals preferably with excitation in the visible window,[6e,9] light-emitting diodes require nanocrystals having large Stokes shift and high quantum efficiency,[1f–g,10] and for solar cells nanocrystals having visible/near-IR (NIR) absorption and/or ternary/quaternary nanocrystals with excess of either of the charge carriers (electron or hole)[1a–d,11] are preferred. So far, no nanocrystal emitters having all such required properties have been reported, and thus further investigations are required to obtain new materials with new properties that would be suitable for versatile applications.

We have now designed a new series of ultrasmall (< 2.5 nm), nearly fixed size, alloyed nanocrystals composed of Cu^{I}–Zn^{II}–In^{III}–Se^{VI} ions which show composition-dependent tunable emissionover most of the visible window. In addition, these nanocrystals are cadmium-free and have aqueous dispersibility, photostability, large Stokes shifts, and high emission intensity (quantum yield (QY) = 25–30 %), which makes them a versatile light-emitting nanoscale materials providing one-step solutions for various applications. The fundamental designing principle of these nanocrystals involves a mechanism whereby composition-variable alloy formation tunes the optical bands from lower to higher energy and vice versa. Here we report details of the synthesis, chemistry of formation, and composition-variable optical tuning of these fixed-size alloy nanocrystals. In addition, aqueous dispersibility and photovoltaic properties of these nanocrystals were investigated.

The alloy nanocrystals were synthesized by simultaneous precipitation and surface cation-exchange protocols. Injection of a selenium precursor into a mixture of Zn^{II}, In^{III}, and Cu^{II} salts at 220 °C (see Experimental Section) results in copper-doped zinc indium selenide alloy nanocrystals whose absorption and emission wavelengths are determined by the In:Zn ratio of the reaction mixture. Further addition of Zn with continuous annealing slowly shifts both absorption and emission bands to the blue in a surface ion-exchange process. Successive photoluminescence (PL) spectra, absorption (UV/Vis) spectra, and a schematic model of surface cation exchange for a typical alloying process are shown in Figure 1 a–c. With an initial Zn:In ratio of 1:2, the emission appears at about 660 nm soon after injection of the Se precursor and is tuned up to 575 nm (Figure 1 a) on introduction of additional Zn precursor, while for an initial Zn:In ratio of 1:1, the emission appears at about 620 nm and is tuned further to the blue, to 540 nm (Figure 1 b), that is, a total

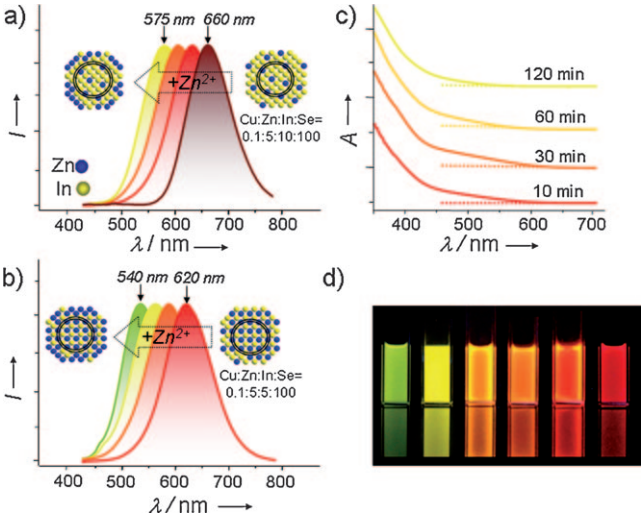

Figure 1. a), b) Typical tunable photoluminescence (PL) spectra during formation of Cu-doped zinc indium selenide and c) tunable UV/Vis spectra of a typical reaction with different In:Zn ratios. Initial Cu:Zn:In:Se ratios in the reaction mixture are inset in (a) and (b). Schematic presentation of internal and surface alloying processes with different In:Zn ratios are also inset in both panels. d) Digital image of samples collected from the reactions of (a) and (b) under UV excitation at 365 nm. *I*: photoluminescence intensity.

[*] S. Sarkar,[+] N. S. Karan,[+] N. Pradhan
Department of Materials Science and Centre for Advanced Materials
Indian Association for the Cultivation of Science
Jadavpur, Kolkata-700032 (India)
E-mail: camnp@iacs.res.in

[+] These authors contributed equally to this work.

[**] This work was supported by DST, India. LNJ Bhilwara Fellowship Foundation and CSIR of India are acknowledged for fellowship. The authors thank Prof. S. K. Dey, Dr. N. R. Jana, and Dr. T. Mishra for their helpful discussion.

Supporting information for this article is available on the WWW under http://dx.doi.org/10.1002/anie.201101572.

window of about 120 nm is covered. The tuning of UV/Vis (Figure 1c) and corresponding PL spectra (Figure 1a) of these alloy nanocrystals clearly indicates composition-dependent variation of the bandgap from low to high energy during the alloying process. Figure 1d shows a digital image of samples with all possible emission colors obtained by variation of both internal and surface In and Zn contents.

To understand the origin of the emission and absorption, the evolution of these optical bands was categorized on the basis of presence/absence of particular element(s) in the reaction mixture. First, the role of Cu, which is present in small amounts (<2% of initial total cation concentration) compared to the other cations, was investigated. Its absence from the reaction mixture does not alter the absorption pattern, but no emission was observed. However, in the absence of any one of In, Zn, and Se, neither such absorption nor emission was observed. This indicates that the host nanocrystals are composed of an alloy of In, Zn, and Se and control the composition-dependent absorption band tuning, while Cu acts as a dopant which is responsible for emission from these alloy nanocrystals. The large Stokes shift (ca. 60 nm), broad nature (full width at half-maximum: 80–115 nm), and long lifetime (ca. 0.3 μm; Supporting Information, Figure S1) of the emission spectra further suggest that the emission is due to the dopant and originates from the Cu center. The emission should not be attributed to Cu-doped ZnSe, as these alloy nanocrystals could be excited even beyond the bulk band of ZnSe (2.7 eV, ca. 465 nm) and Cu-doped ZnSe does not emit within this range.[6c] Even though we used Cu^{II} salts in the reaction mixture, the absence of a characteristic Cu^{II} signal in the EPR spectrum suggests that Cu is in oxidation state of +1. Conversion of Cu^{II} to Cu^{I} during the doping process[12] and/or in the presence of fatty amines[13] was proposed in the literature. Hence, the tunable dopant emission here is expected to be due to the exciton generated from the ternary host zinc indium selenide nanocrystals, which recombines through Cu^{I} d states.[14]

Apart from variation of composition, tuning of the optical bands observed with progress of the reaction could also be due to variations in the size of the nanocrystals, which is well known to control the bandgap in quantum-confined nanocrystals.[2] To rule out this possibility, size and composition of samples at various stages of the reaction were measured. The TEM images in Figure 2a and b show that the size of the nanocrystals remains almost same throughout the reaction (2.1 ± 0.2 nm; Supporting Information, Figure S2) but their composition, measured by inductively coupled plasma atomic emission spectroscopy (ICP-AES), changes successively. Since the Zn content of the nanocrystals increases with progressing reaction, while the size of nanocrystals remains constant throughout the reaction, we assume that Zn continuously replaces In in the outer layer of the nanocrystals. As ZnSe (bulk bandgap: 2.7 eV) has a larger bandgap than In_2Se_3 (bulk bandgap: 1.8 eV), a higher Zn:In ratio shifts the absorption and emission position bands of the alloy nanocrystals to the blue. To further confirm this, powder XRD patterns of samples at different stages (Figure 2c) were measured to understand the composition-dependent tuning of the optical bands. Detailed analysis of the XRD data revealed that the alloy has the characteristics of zinc blende (ZB) ZnSe. When indium selenide was synthesized with Cu^{I} as dopant (<2% of total In concentration) in a control reaction without zinc precursor by following a similar reaction protocol, no XRD peak was obtained from the sample. This suggests that the indium selenide formed here is probably amorphous in nature, and hence our observed XRD peaks are compared with bulk ZB ZnSe. The corresponding XRD peaks of the samples with higher In:Zn ratio shift to lower angle compared to ZB ZnSe, because of substitution of smaller Zn^{2+} ($r = 0.88$ Å) by larger In^{3+} ($r = 0.94$ Å). The fractions of In and Zn in samples having different emission wavelength, measured by ICP-AES, are indicated in Figure 2c for clear comparison.

To further understand the evolution and tuning of the dopant emission through surface cation exchange during the entire alloying process, X-ray photoelectron spectroscopy (XPS) measurements were carried out at different stages of a reaction. The XPS measurements showed Zn:In ratios of 0.25:1 and 9:1 at the initial (emission center at 650 nm) and final (emission center at 590 nm) stages of the reaction

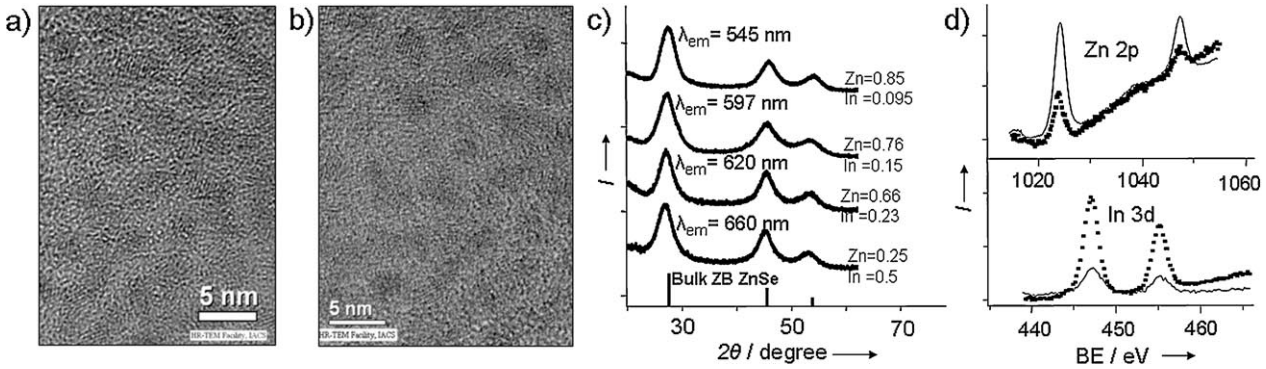

Figure 2. a), b) TEM images of the sample taken before and after injection of additional Zn precursor. c) XRD patterns during the surface alloying process. The indicated fractions of Zn and In were determined by ICP-AES. The amount of Cu was less than 1% of total Zn and In in all cases. d) XPS of initial and final samples during the surface alloying process. The Zn:In ratios before and after surface alloying were calculated with Casa software and values are reported in the text. All measurements were carried out on samples from the reactions of Figure 1a and b. *I*: intensity. In (d) the solid line represents the final sample, and the dotted line the initial sample. BE: binding energy.

(Figure 2d), but ICP-AES analysis of the sample showed 0.7:1 and 9.8:1 respectively. The XPS data clearly show that the Zn:In ratio is greatly increased in the final compared to the initial stage of the reaction, but the ICP-AES analysis does not show such high enhancement of this ratio. The XPS measurements, which are sensitive to the surface, confirm that most of the In ions from the surface of the nanocrystals are replaced by Zn ions. Further addition of Zn precursor and annealing for a longer time do not help to tune the emission below 575 nm. This indicates that the inner core composition remains the same and mostly the surface composition changes with progressing reaction. Hence, once maximum replacement of surface cations (In) has occurred, further addition of Zn does not alter the emission position. This suggests that the composition tunability during the reaction (i.e., after addition of Zn) is mostly controlled by cation exchange at the surface layer of the nanocrystals, which tunes the optical bands, whereas the initial position of the optical band is mainly governed by the initial stoichiometry in the reaction mixture. However, the overall tuning is governed by both the initial ratio of precursors and the surface cation-exchange process. Hence, for long-range tuning, more than one reaction must be performed, and though this may be seen as a demerit of the system, it provides a clear view of the chemistry of internal and surface composition variation during the reaction.

Next, we investigated the fixed and restricted diameter (2.1 ± 0.2 nm) of the nanocrystals during the alloying process. For the whole range of tunability (Figure 1a or b), the reaction must be continued for hours. The necessary prolonged reaction was designed with proper manipulation of reaction parameters, reagent concentration, and suitable capping ligands to slow down the cation-exchange process. With excess of In, the reaction mixture turns colloidal immediately after injection of the Se precursor. The TEM image of this colloidal sample (Supporting Information, Figure S3) indicates formation of faceted or anisotropically shaped nanocrystals, which is typically due to the excess In content. To prevent this, the reaction was carried out with optimized In content at a suitable reaction temperature with an excess of strongly binding ligands such as long-chain alkyl thiols and long-chain fatty amines. Trioctylphosphine (TOP) was also used for long-term dispersity of these nanocrystals in solution.[6d] In the entire reaction process, thiols act as growth inhibitor ligands owing to their restricted dynamicity on the surface of nanocrystals, and the ideally designed reaction conditions control the slow cation-exchange alloying process. Hence, the average diameter of the nanocrystals is restricted to 2.5 nm, even after annealing for more than two hours.

Ternary nanocrystals involving In and Cu have already been reported in the literature, and Cu–In–S (or Se) nanocrystals are well known.[6d–e,7e,15] However, these are not Cu-doped but a homogeneous mixture of Cu, In, and S (or Se) with significant amount of Cu and have different crystal structure with different photophysical properties. Recently, Peng et al. reported tunable emission (500–950 nm) from $CuInS_2$ with ZnS shell, which grows up to 20 nm. This represents optical-band tuning from higher to lower energy as the nanocrystal grows, and is similar to other reports on Cu–In–S.[6d] Most importantly, the optical spectral tuning is mainly controlled by the content of In and Cu in the nanocrystal. Similarly, Cu–Zn–In–S was also reported with low quantum yield and short-range tunability from higher to lower energy window with increasing nanocrystal size.[7e,16] Bawendi et al. also reported Cu–In–Se nanocrystals which mostly emit in the NIR window, but the nature and stability of emission have not been clarified.[15a] Recently Cu-doped InP has been reported with ZnSe diffusion barrier, which emits in the red-to-IR window.[17] Nevertheless, the current designed nanocrystals are unique in retaining their small fixed size while the emission is tuned from lower to higher energy over most of the visible window, and thus provide a clear mechanism of composition-dependent bandgap tuning. Hence, these nanocrystals are different from $CuInS_2$ and $CuInSe_2$[6d,e,7e,15] nanocrystals with respect to their physical dimensions, chemical composition, and photophysical properties.

While optical tuning in semiconductor nanocrystals mostly takes place from higher to lower energy during annealing and growth,[2] we observed composition-dependent tuning from lower to higher energy bands. Interestingly, it can also be tuned from higher to lower energy by using an appropriate In:Zn ratio followed by the cation exchange of Zn with In. This makes our system more flexible for selecting the initial absorption and emission and their tuning to either side of the spectrum, by overcoming the chemical reactivity barriers of In and Zn cations. As per chemical reactivity, one-way cation exchange is possible because of the allowed free-energy changes, but at higher temperature in nonpolar solvent, where ions are mostly covalently bonded, this principle may not be strictly followed. As the tunability of optical bands is mostly governed by surface cation-exchange, and a particular cation (Zn or In) present in higher content in the reaction mixture replaces the other cation present on the surface of the nanocrystals, it can be assumed here that the feasibility of ion replacement is mostly controlled by bulk cation population rather than chemical reactivity. Even in a single set of reactions in which the bulk cation concentration is varied, the emission can be tuned back and forth (see Supporting Information, Figure S4), which further supports our assumption. However, in either case, the tunability is restricted to a small spectral window, which suggests that cation replacement occurs only at the surface. When we tried to replace the core cations by increasing the reaction temperature, the reaction mixture turned colloidal and mixtures of nanocrystals were obtained with several new nuclei. Hence, we can conclude that the entire process of ion exchange restricted to the surface of nanocrystals is driven by the excess monomer concentration present in the bulk solution.

The ultrasmall green-, yellow-, and red-emitting nanocrystals were explored in different applications. They were functionalized with polyacrylamine and mercaptopropionic acid ligands (Supporting Information, Figure S5) and found to be stable while dispersed in water. As the nanocrystals are cadmium-free, ultrasmall, and can be excited in the visible window, these would be a suitable candidate for different biological applications after proper surface functionalization. In spite of the small dimensions, the nanocrystals are stable for months without aggregation. We also carried out photocurrent measurements on these Cu-doped ternary alloy

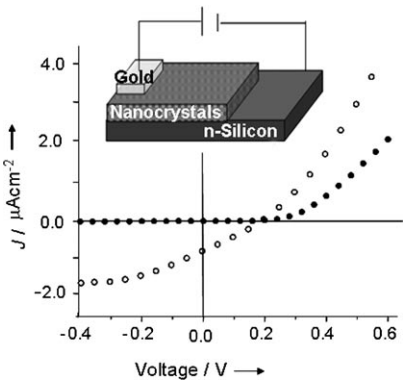

Figure 3. *I–V* characteristics of a p–n junction involving Cu-doped Zn–In–Se nanocrystals and n-silicon in the presence of light (80 mW cm^{-2}) and in the dark. Inset: sketch of the device for *I–V* measurements. *J*: current density. Empty and filled circles represent the measurements in the presence and absence of light, respectively. Details of the measurements are provided in the Supporting Information.

nanocrystals showing visible-window excitation. Figure 3 shows the *I–V* characteristics of a thin film of nanocrystals in the dark and in the presence of light. The observed rectification behavior suggests that these materials can be used for photovoltaics. In addition, they have large Stokes shift (minimum reabsorption/interparticle energy transfer) and can be used as an efficient materials in LEDs.

In summary, we have reported the synthesis of stable, ultrasmall (size <2.5 nm), cadmium-free, Cu-doped Zn^{II}–In^{III}–Se^{VI} ternary alloy nanocrystals by simultaneous precipitation and surface cation-exchange protocols. The size of these doped ternary nanocrystals remains unchanged throughout the alloying process. By varying the surface composition at fixed size, we achieved emission covering most of the visible window (ca. 660–540 nm). The bandgap can be reversibly tuned from low to high energy and vice versa by simply changing the ratio of the cations in the reaction mixture. In addition, these ultrasmall nanocrystals have versatile characteristics which would meet the demands of biomedical, solar cell, and LED applications.

Experimental Section

Synthesis of Cu-doped Zn–In–Se nanocrystals: 0.05 mmol of Zn stearate ($ZnSt_2$) and 0.5 mL of indium acetate stock solution (1 mmol of indium acetate in 10 mmol of oleic acid, ODE added to give total volume of 10 mL) with 4 mL of 1-octadecene (ODE), 2 mL of 1-dodecanethiol (DDT,) and 1 mL of trioctylphosphine (TOP) were loaded into a 25 mL three-necked round-bottom flask and degassed for 15 min with argon. Then the temperature was raised to 220 °C and 0.5 mL of TBP/Se solution (23.17 mmol of Se in 10 mL of tributylphosphine, TBP) with 2.0 mmol 1-octadecylamine (ODA) was injected, followed by addition of 0.05 mL of Cu stock solution (0.1 mmol of $CuCl_2$ in 5 mL of oleylamine). The reaction mixture was annealed at the same temperature and monitored through UV/Vis and photoluminescence spectra. Then, the entire stock solution of $ZnSt_2$ was injected in 0.5 mL portions at intervals of 15 min at the same reaction temperature. Samples were collected for photoluminescence and absorption measurements during further annealing. Nanocrystals were purified by using acetone as nonsolvent and dispersed in chloroform. The Cu source can also be introduced at the beginning along with In and Zn in the reaction mixture.

Received: March 3, 2011
Published online: May 13, 2011

Keywords: doping · luminescence · nanoparticles · semiconductors · zinc indium selenide

[1] a) J. H. Bang, P. V. Kamat, *ACS Nano* **2009**, *3*, 1467 – 1476; b) S. Dayal, N. Kopidakis, D. C. Olson, D. S. Ginley, G. Rumbles, *Nano Lett.* **2010**, *10*, 239 – 242; c) W. Ma, J. M. Luther, H. Zheng, Y. Wu, A. P. Alivisatos, *Nano Lett.* **2009**, *9*, 1699 – 1703; d) C. Steinhagen, M. G. Panthani, V. Akhavan, B. Goodfellow, B. Koo, B. A. Korgel, *J. Am. Chem. Soc.* **2009**, *131*, 12554 – 12555; e) P. O. Anikeeva, J. E. Halpert, M. G. Bawendi, V. Bulovic, *Nano Lett.* **2009**, *9*, 2532 – 2536; f) V. L. Colvin, M. C. Schlamp, A. P. Alivisatos, *Nature* **1994**, *370*, 354 – 357; g) M. A. Schreuder, K. Xiao, I. N. Ivanov, S. M. Weiss, S. J. Rosenthal, *Nano Lett.* **2010**, *10*, 573 – 576; h) M. Bruchez, Jr., M. Moronne, P. Gin, S. Weiss, A. P. Alivisatos, *Science* **1998**, *281*, 2013 – 2016; i) W. C. Chan, S. Nie, *Science* **1998**, *281*, 2016 – 2018; j) X. Gao, Y. Cui, R. M. Levenson, L. W. K. Chung, S. Nie, *Nat. Biotechnol.* **2004**, *22*, 969 – 976.

[2] C. B. Murray, D. J. Norris, M. G. Bawendi, *J. Am. Chem. Soc.* **1993**, *115*, 8706 – 8715.

[3] a) Z. A. Peng, X. Peng, *J. Am. Chem. Soc.* **2001**, *123*, 183 – 184; b) L. Qu, Z. A. Peng, X. Peng, *Nano Lett.* **2001**, *1*, 333 – 337; c) A. Yang Yongan, H. Wu, R. Williams Kathryn, Y. C. Cao, *Angew. Chem.* **2005**, *117*, 6870 – 6873; *Angew. Chem. Int. Ed.* **2005**, *44*, 6712 – 6715.

[4] a) D. V. Talapin, A. L. Rogach, A. Kornowski, M. Haase, H. Weller, *Nano Lett.* **2001**, *1*, 207 – 211; b) P. Reiss, J. Bleuse, A. Pron, *Nano Lett.* **2002**, *2*, 781 – 784.

[5] a) T. Pellegrino, L. Manna, S. Kudera, T. Liedl, D. Koktysh, A. L. Rogach, S. Keller, J. Raedler, G. Natile, W. J. Parak, *Nano Lett.* **2004**, *4*, 703 – 707; b) S.-W. Kim, S. Kim, J. B. Tracy, A. Jasanoff, M. G. Bawendi, *J. Am. Chem. Soc.* **2005**, *127*, 4556 – 4557.

[6] a) R. N. Bhargava, D. Gallagher, X. Hong, A. Nurmikko, *Phys. Rev. Lett.* **1994**, *72*, 416 – 419; b) D. J. Norris, N. Yao, F. T. Charnock, T. A. Kennedy, *Nano Lett.* **2001**, *1*, 3 – 7; c) N. Pradhan, D. Goorskey, J. Thessing, X. Peng, *J. Am. Chem. Soc.* **2005**, *127*, 17586 – 17587; d) R. Xie, M. Rutherford, X. Peng, *J. Am. Chem. Soc.* **2009**, *131*, 5691 – 5697; e) L. Li, T. J. Daou, I. Texier, T. T. Kim Chi, N. Q. Liem, P. Reiss, *Chem. Mater.* **2009**, *21*, 2422 – 2429; f) D. Battaglia, X. Peng, *Nano Lett.* **2002**, *2*, 1027 – 1030.

[7] a) R. E. Bailey, S. Nie, *J. Am. Chem. Soc.* **2003**, *125*, 7100 – 7106; b) M. Wang, G. T. Fei, Y. G. Zhang, M. G. Kong, D. Z. Li, *Adv. Mater.* **2007**, *19*, 4491 – 4494; c) Z. Deng, H. Yan, Y. Liu, *J. Am. Chem. Soc.* **2009**, *131*, 17744 – 17745; d) D. Pan, X. Wang, Z. H. Zhou, W. Chen, C. Xu, Y. Lu, *Chem. Mater.* **2009**, *21*, 2489 – 2493; e) H. Nakamura, W. Kato, M. Uehara, K. Nose, T. Omata, S. Otsuka-Yao-Matsuo, M. Miyazaki, H. Maeda, *Chem. Mater.* **2006**, *18*, 3330 – 3335; f) X. Zhong, M. Han, Z. Dong, J. White Timothy, W. Knoll, *J. Am. Chem. Soc.* **2003**, *125*, 8589 – 8594.

[8] a) A. P. Alivisatos, *J. Phys. Chem.* **1996**, *100*, 13226 – 13239; b) J. E. Murphy, M. C. Beard, A. G. Norman, S. P. Ahrenkiel, J. C. Johnson, P. Yu, O. I. Micic, R. J. Ellingson, A. J. Nozik, *J. Am. Chem. Soc.* **2006**, *128*, 3241 – 3247; c) H. Htoon, A. V. Malko, D. Bussian, J. Vela, Y. Chen, J. A. Hollingsworth, V. I. Klimov, *Nano Lett.* **2010**, *10*, 2401 – 2407.

[9] a) J. P. Zimmer, S. W. Kim, S. Ohnishi, E. Tanaka, J. V. Frangioni, M. G. Bawendi, *J. Am. Chem. Soc.* **2006**, *128*, 2526 – 2527; b) C. Kirchner, T. Liedl, S. Kudera, T. Pellegrino, A. M. Javier, H. E. Gaub, S. Stoelzle, N. Fertig, W. J. Parak, *Nano Lett.* **2005**, *5*, 331 –

338; c) T. Pons, E. Pic, N. Lequeux; E. Cassette, L. Bezdetnaya, F. Guillemin, F. Marchal, B. Dubertret, *ACS Nano* **2010**, *4*, 2531 – 2538; E. Cassette, L. Bezdetnaya, F. Guillemin, F. Marchal, B. Dubertret, *ACS Nano* **2010**, *4*, 2531 – 2538.

[10] a) A. L. Rogach, N. Gaponik, J. M. Lupton, C. Bertoni, D. E. Gallardo, S. Dunn, N. Li Pira, M. Paderi, P. Repetto, S. G. Romanov, C. O'Dwyer, C. M. Sotomayor Torres, A. Eychmueller, *Angew. Chem.* **2008**, *120*, 6638 – 6650; *Angew. Chem. Int. Ed.* **2008**, *47*, 6538 – 6549; b) A. K. Rath, S. Bhaumik, A. J. Pal, *Appl. Phys. Lett.* **2010**, *97*, 113502.

[11] Q. Guo, S. J. Kim, M. Kar, W. N. Shafarman, R. W. Birkmire, E. A. Stach, R. Agrawal, H. W. Hillhouse, *Nano Lett.* **2008**, *8*, 2982 – 2987.

[12] a) A. V. Isarov, J. Chrysochoos, *Langmuir* **1997**, *13*, 3142 – 3149; b) C. Corrado, Y. Jiang, F. Oba, M. Kozina, F. Bridges, J. Z. Zhang, *J. Phys. Chem. A* **2009**, *113*, 3830 – 3839.

[13] J. Tang, G. Konstantatos, S. Hinds, S. Myrskog, A. G. Pattantyus-Abraham, J. Clifford, E. H. Sargent, *ACS Nano* **2009**, *3*, 331 – 338.

[14] a) P. Peka, H. J. Schulz, *Solid State Commun.* **1994**, *89*, 225 – 228; b) B. B. Srivasatava, S. Jana, N. Pradhan, *J. Am. Chem. Soc.* **2011**, *133*, 1007 – 1015.

[15] a) P. M. Allen, M. G. Bawendi, *J. Am. Chem. Soc.* **2008**, *130*, 9240 – 9241; b) J. J. Nairn, P. J. Shapiro, B. Twamley, T. Pounds, R. von Wandruszka, T. R. Fletcher, M. Williams, C. Wang, M. G. Norton, *Nano Lett.* **2006**, *6*, 1218 – 1223; c) M. A. Malik, P. O'Brien, N. Revaprasadu, *Adv. Mater.* **1999**, *11*, 1441 – 1444; d) J. Xiao, Y. Xie, Y. Xiong, R. Tang, Y. Qian, *J. Mater. Chem.* **2001**, *11*, 1417 – 1420; e) E. Cassette, T. Pons, C. Bouet, M. Helle, L. Bezdetnaya, F. Marchal, B. Dubertret, *Chem. Mater.* **2010**, *22*, 6117 – 6124.

[16] S. Shen, L. Zhao, Z. Zhou, L. Guo, *J. Phys. Chem. C* **2008**, *112*, 16148 – 16155.

[17] R. Xie, X. Peng, *J. Am. Chem. Soc.* **2009**, *131*, 10645 – 10651.

